the structure of Cu_4O in Fig. 7(*b*) and that of α-$Cu_4O_{0.75}$ in Fig. 8(*b*) that the crystal planes (140) and (200) in α-$Cu_4O_{0.75}$ correspond to those of (120) and (200) in Cu_4O, which consist of Cu atoms, and the crystal plane of (120) in α-$Cu_4O_{0.75}$ corresponds to that of (110) in Cu_4O, which consists of O atoms. From Fig. 14 it can be seen that the amplitudes of the diffracted waves of (140) and (200) in α-$Cu_4O_{0.75}$, which reflect the periodicity of the arrangement of copper, vary with the film thickness at a periodicity of about 7 nm; in contrast, the amplitudes of the diffracted waves of (120), which reflect the periodicity of the arrangement of O, simply increase with the film thickness up to about 50 nm. Thus, when the film thickness becomes of a large-enough value, where the amplitude of (120) is larger than that of (140) and (200), the intensity of the imaging spots of O atoms will be stronger than those of Cu atoms. Similar arguments (based on Fig. 14 and the models shown in Figs. 10 and 12 respectively) hold for the structures of β- and γ-$Cu_4O_{0.75}$.

The present authors thank Drs M. Tomita and Y. Yokota and Mr Inada for their help in preparing this manuscript.

References

GUAN, R., HASHIMOTO, H. & KUO, K. H. (1984). *Acta Cryst.* **B40**, 560–566.
GUAN, R., HASHIMOTO, H. & KUO, K. H. (1985). *Acta Cryst.* **B41**, 219–225.
GUAN, R., HASHIMOTO, H. & KUO, K. H. (1986). *Ultramicroscopy*, **20**, 195–202.
GUAN, R., HASHIMOTO, H. & KUO, K. H. & YOSHIDA, T. (1987). *Acta Cryst.* **B43**, 343–346.
GUAN, R., HASHIMOTO, H. & YOSHIDA, T. (1984). *Acta Cryst.* **B40**, 109–114.

Acta Cryst. (1990). **B46**, 111–117

Electron Microscopy Study of the Incommensurately Modulated Structure of Ankangite

BY X. J. WU AND F. H. LI

Institute of Physics, Chinese Academy of Sciences, Beijing 100080, *People's Republic of China, and Beijing Laboratory of Electron Microscopy, Beijing* 100080, *People's Republic of China*

AND H. HASHIMOTO

Faculty of Engineering, Okayama University of Science, Okayama 700, *Japan*

(*Received* 10 *July* 1989; *accepted* 27 *November* 1989)

Abstract

The one-dimensional incommensurately modulated structure of ankangite $[Ba_{0.827}(Ti_{5.827}V_{2.294}Cr_{0.053})O_{16}]$, a mineral recently discovered in China, has been studied by electron diffraction and high-resolution electron microscopy. Its average structure is tetragonal with lattice parameters $a = 10.2$ and $c = 2.96$ Å and possible space groups $I4$, $I\bar{4}$ and $I4/m$. The modulated wave spreading along the c axis has wavelength $\lambda = 2.30c$. By referring to the results of the electron diffraction analysis it is suggested that the existence of a large number of vacancies inside tetragonal channels makes the Ba ions deviate from their idealized positions to form the modulated structure. Diffuse diffraction streaks passing through satellite spots were observed and hence modulation waves through adjacent Ba-ion strings are considered to be incoherent. This was confirmed by high-resolution electron microscopy and optical diffraction. The effect of electron-beam irradiation on the structure of ankangite is reported.

1. Introduction

Ankangite $[Ba_{0.827}(Ti_{5.827}V_{2.294}Cr_{0.053})O_{16}]$ is a new mineral recently discovered in China. Its chemical formula is close to that of priderite. The crystal structure of ankangite was also considered to be similar to that of priderite (Zhou & Ma, 1987), which is isomorphous to hollandite. The crystal structure of hollandite has been determined by X-ray diffraction (Bystrom & Bystrom, 1950, 1951). Fig. 1 shows a structure model of hollandite projected along the c axis (Bystrom & Bystrom, 1950). In the structure of hollandite MO_6 octahedra (where M represents Mn and its substitutes) share edges along the c axis, forming strings which are linked by corner-sharing and edge-sharing to form tetragonal channels with

0108-7681/90/020111-07$03.00

cations inside. There must be some vacancies in the cation positions in hollandite because the number of cations is much lower than the number of positions in the channels at which the cations can be located. Dryden & Wadsley (1958) studied hollandite of composition $Ba_xMg_xTi_{8-x}O_{16}$ ($0{\cdot}67 < x < 1{\cdot}14$) by X-ray single-crystal diffraction. They suggested that the occupancy of the tetragonal channels can be presented as Ba–vacancy–Ba–vacancy but that some channels contain long strings of empty sites or can be completely empty. Some diffuse streaks observed in an X-ray diffractograph were considered to be due to the shape factor which results from the positional incoherency of adjacent Ba-ion strings. Beyeler (1976) also observed X-ray diffuse scattering in a hollandite of composition $K_{1{\cdot}54}Mg_{0{\cdot}77}Ti_{7{\cdot}23}O_{16}$. This was interpreted as the consequence of both the deviation of cations from their standard positions along tetragonal channels and the incoherency of cation strings in different channels. The displacement of cations along the c axis has also been discussed by Sinclair, McLaughlin & Ringwood (1980) and Post & Burnham (1986). Post, Von Dreele & Buseck (1982) proposed that other atoms are also displaced so that the tetragonal symmetry degenerates to monoclinic. Bursill & Grzinic (1980) studied samples of hollandite with the compositions $Ba_xTi_{8-x}Mg_xO_{16}$ and $Ba_xTi_{8-2x}Ga_{2x}O_{16}$ by electron diffraction and high-resolution electron microscopy. Sharp satellite diffraction spots, irrational to the main diffraction peaks, were observed in the electron diffraction patterns. They proposed that hollandite may have a commensurately or an incommensurately modulated structure depending on the value of x, and that the period of the modulated structure also depends on the value of x. In addition, they proposed a local ordered intergrowth model of Ba atoms to explain the modulated structure.

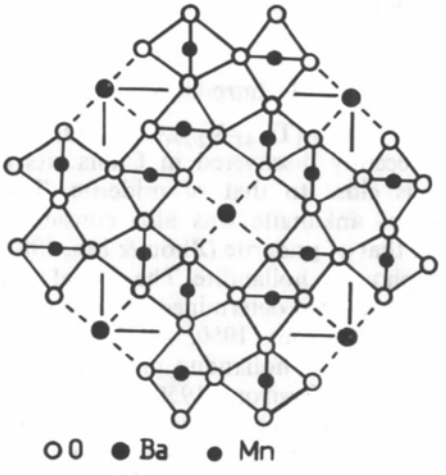

Fig. 1. Projection of the structure model of hollandite along the c axis (Bystrom & Bystrom, 1950).

Zhou & Ma (1987) reported that for ankangite there are, in addition to the main diffraction peaks, satellite diffraction peaks arranged along directions parallel to the c axis. The ratio of the period of the main spots to the period of the satellite spots is non-integral and about 2·27. Based on this phenomenon they supposed that ankangite has one-dimensional incommensurate superlattice ordering along the c axis. They also discussed the crystal structure of ankangite with reference to the structure models of hollandite proposed by Dryden & Wadsley (1958) and Bursill & Grzinic (1980). The average subcell determined from the main diffraction spots is tetragonal with parameters $a = 10{\cdot}118$, $c = 2{\cdot}956$ Å and possible space groups $I4/m$, $I4$ and $I\bar{4}$.

In the present paper studies of ankangite by electron diffraction, high-resolution electron microscopy and optical diffraction are reported.

2. Experimental

Samples of ankangite were ground in an agate mortar to give fine-fractured particles. The particles were dispersed in alcohol and a drop of the resultant suspension was placed on a microgrid, which was covered with an evaporated thin foil of gold for calibrating the electron diffraction camera length.

EM-420 and JEM-200CX transmission electron microscopes were used for obtaining the electron diffraction patterns and high-resolution images, respectively. Optical diffractograms were taken of some images using an LD-10 optical diffractometer.

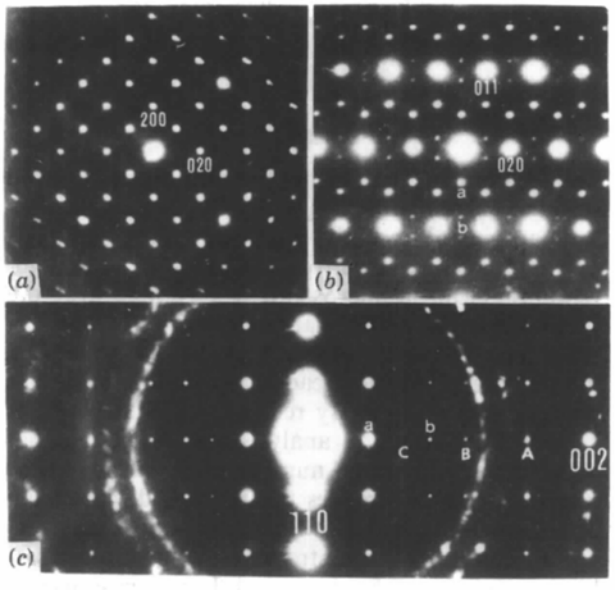

Fig. 2. Electron diffraction patterns of ankangite. Incident electron beam parallel to (*a*) [001], (*b*) [100] and (*c*) [1$\bar{1}$0]. Satellite diffraction spots arranged along directions parallel to the c axis can be seen in (*b*) and (*c*).

3. Lattice parameters and possible space groups of the average structure

Figs. 2(*a–c*) are electron diffraction patterns (EDP's) taken along directions [001], [100] and [1$\bar{1}$0], respectively. The lattice parameters of the average tetragonal structure can be determined from Fig. 2(*a*) and from the strong (main) spots in Figs. 2(*b*) and 2(*c*). They are $a = 10{\cdot}2$ and $c = 2{\cdot}96$ Å. The modulated wavevector is parallel to the c axis and the basic vector of the modulated wave $\mathbf{q} = \mathbf{c}^*/2{\cdot}30$. All main reflections with $h + k + l =$ odd are prohibited by extinction rules. Hence, the possible space groups of the average structure are $I4$, $I\bar{4}$ and $I4/m$. These results are in agreement with those obtained by X-ray diffraction (Zhou & Ma, 1987).

4. Satellite spots and diffraction streaks

The weak spots in Figs. 2(*b*) and 2(*c*) are satellite diffraction spots; for instance, the spots labelled *a* and *b* in Figs. 2(*b*) and 2(*c*) are the first- and second-order satellite spots, respectively, belonging to the center spot. Likewise, the spots labelled *A*, *B* and *C* in Fig. 2(*c*) are the first-, second- and third-order satellite spots, respectively, of the main (002) diffraction.

A series of EDP's taken along different zone axes were obtained by tilting the sample around its *b* axis and are shown in Fig. 3. In order to index all spots in these EDP's four indices h, k, l, m must be used (de Wolff, 1974).

Weak diffraction streaks running along the b^* axis were observed as shown by the arrows *R* and *S* in Fig. 3. The weak streaks always pass through satellite spots when the latter appear in the EDP's. The existence of the streaks in all EDP's implies that the streaks form a group of continuous planes in reciprocal space, parallel to a^*b^* and passing through the satellite spots. Fig. 4 is a schematic diagram of the a^*c^* plane in reciprocal space. The filled circles are the reciprocal lattice points corresponding to the main diffraction spots and the open circles are their first-order satellites ($m = \pm 1$). The two satellite spots belonging to the main spot 200 are indicated by bold arrows. The dashed lines passing through the satellite spots are the loci of the vertical reciprocal continuous planes intersected with the plane a^*c^*. The five solid lines labelled *a*, *b*, *c*, *d* and *e* indicate the loci of the sphere of reflection intersected with the a^*c^* plane for [100], [10$\bar{1}$], [10$\bar{2}$], [10$\bar{3}$] and [10$\bar{4}$] incidences, respectively, of the electron beam. When the electron beam is incident along the [100] direction (Fig. 3*a*), the sphere of reflection cuts all reciprocal continuous planes to give the streak pairs passing through satellite spots. When the electron beam is not perpendicular to the c axis (Figs. 3*b–e*), the sphere of reflection does not generally meet any satellite spots. Conversely, it may meet a few satellite spots when the lattice points are elongated into

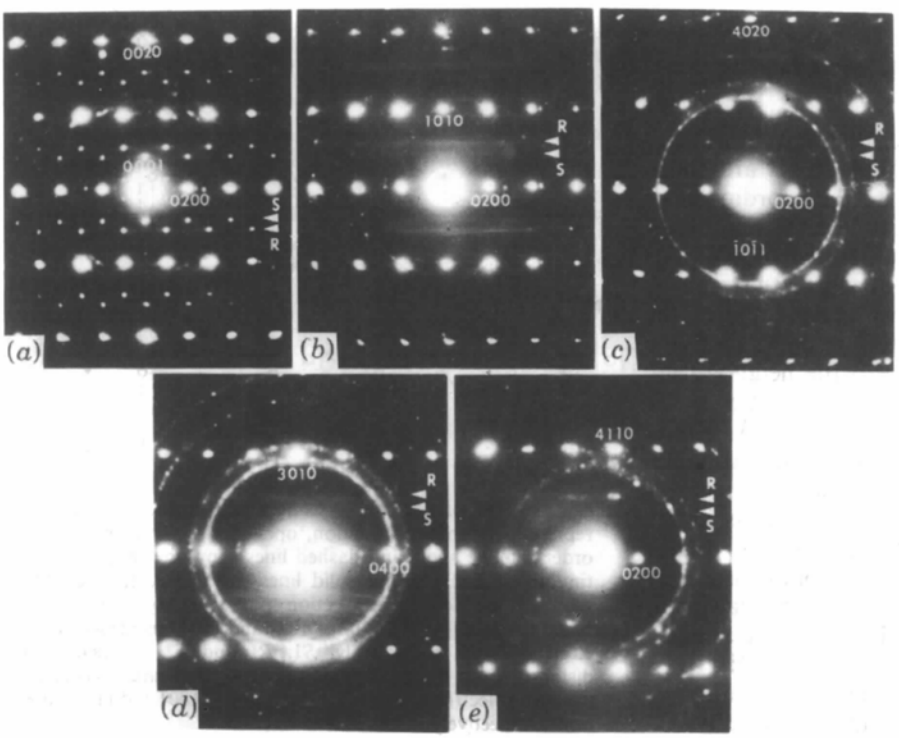

Fig. 3. A series of electron diffraction patterns taken by tilting the crystal around [010]. Incident electron beam parallel to (*a*) [100], (*b*) [10$\bar{1}$], (*c*) [10$\bar{2}$], (*d*) [10$\bar{3}$] and (*e*) [10$\bar{4}$]. The weak diffraction streaks are indicated by the arrows *R* and *S*.

spikes owing to the plate-like shape of the crystals, but it always intersects the reciprocal continuous planes. Obviously, the ratio of the distances from the center spot to the nearest streak pair for all incidences R_j/S_j should always remain constant. This was confirmed by the experimental measurements.

When the electron beam is incident along the $[10\bar{2}]$ direction, the weak satellite spots $101\bar{1}$ and $\bar{1}0\bar{1}1$ can be seen in Fig. 3(*c*). In this case, the solid line *c*, which represents the section of the sphere of reflection with the reciprocal lattice, does not strictly meet satellite spots $10\bar{1}\bar{1}$ and $\bar{1}0\bar{1}1$ as shown in Fig. 4. Because of the shape factor of the thin plate-like crystals, all reciprocal lattice points are elongated along the direction normal to the plate and form reciprocal lattice spikes. Therefore, the weak satellite diffraction spots $\bar{1}0\bar{1}1$ and $101\bar{1}$ appear when the solid line *c* crosses the reciprocal satellite lattice spikes.

5. Displacive incommensurately modulated structure caused by cation vacancies

It is well known that there are two main mechanisms by which incommensurately modulated structures are formed – compositional and displacive modulation.

The structure factor of a pure compositional modulation in four-dimensional space can be expressed as (de Wolff, 1974):

$$F(hklm) = \sum_j \exp[2\pi i(hx_j + ky_j + lz_j)] \times \int_0^1 f_j(u)\exp(2\pi imu)\mathrm{d}u. \quad (1)$$

$f_j(u)$ is a continuous periodic function in fourth-dimensional space where the hyperatoms are continuously distributed; (x_j, y_j, z_j) are the coordinates of the *j*th atom. In the case of ankangite the number of Ba ions is much lower than the number of positions inside the tetragonal channels at which they can be located. In the ideal structure of ankangite, the coordination number of Ba ions is eight, and the average distance from a Ba ion to the neighbouring oxygen atoms is about 3·00 Å, but the sum of the ionic radii of Ba and O is only about 2·78 Å. Therefore, the Ba ions may be displaced in the tetragonal channels within certain limits. The existence of vacancies and the displacement of Ba atoms in the tetragonal channels are considered to be two major reasons for the formation of an incommensurately modulated structure in ankangite. The displacement of Ba atoms may also cause other atoms, especially oxygen atoms, to have some but smaller displacement. Atoms other than Ba and O may be negligibly displaced or may arrange periodically. To a first approximation it can be assumed that for ankangite only Ba atoms contribute to the incommensurate modulation of the crystal structure. Then, the structure factor of (1) can be divided into two parts F_1 and F_2, $F_1(hklm)$ only being related to the Ba atoms, while $F_2(hkl)$ is related to all other atoms. When $m \neq 0$, namely, for satellite spots

$$F(hklm) = F_1(hklm) = f_{\mathrm{Ba}}\sum_j \exp[2\pi i(x_j h + y_j k + z_j l) \times \int_0^1 T(u)\exp(2\pi imu)\mathrm{d}u = \gamma_m F_1(hkl0). \quad (2)$$

Here $T(u)$ is a normalized periodic function,

$$\gamma_m = \int_0^1 T(u)\exp(2\pi imu)\mathrm{d}u,$$

which depends only on *m*. Hence,

$$F(hklm)/F(000m) = F_1(hkl0)/F_1(0000). \quad (3)$$

Formula (3) implies that the intensity of satellite spots corresponding to the transmission beam would be stronger or much stronger than that corresponding to the main diffraction beams. It seems from the EDP's given in Figs. 2(*c*) and 3(*a*) that such an argument is not valid for ankangite.

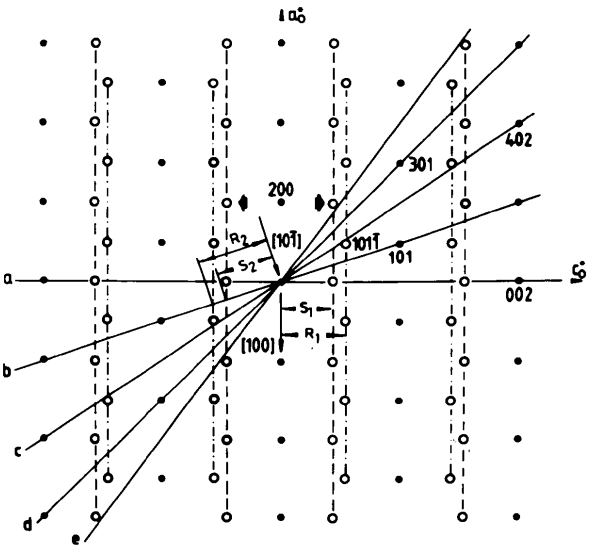

Fig. 4. Sketch of a^*c^* cross-section in reciprocal space. Dots represent the main diffraction, open circles represent the first-order satellite spots and dashed lines show the reciprocal continuous planes. The five solid lines, labelled *a*, *b*, *c*, *d* and *e*, represent the loci of the reflection sphere intersected by the a^*c^* plane for [100], [10$\bar{1}$], [10$\bar{2}$], [10$\bar{3}$] and [10$\bar{4}$] incidences of the electron beam, respectively. *S*1, *R*1 and *S*2, *R*2 denote the distances from the transmission spot to the nearest streak pair when the electron beam is incident along [100] and [10$\bar{1}$] directions, respectively.

The atomic position in a displacive modulated structure can be expressed as:

$$\mathbf{r}_j = \mathbf{r}_{0j} + \mathbf{u}_j. \quad (4)$$

Here $\mathbf{r}_{0j}$ denotes the average position of the jth atom and $\mathbf{u}_j$ denotes the periodic displacement function. The structure factor of a displacive modulated structure can be written as (Steeds, Bird, Eaglesham, Mckernan, Vincent & Withers, 1985; Axe, 1980)

$$F(hklm) = \sum_j f_j \exp(2\pi i \mathbf{g}\mathbf{r}_j). \quad (5)$$

The expression, $\mathbf{g} = \mathbf{H} + m\mathbf{q} = h\mathbf{a}^* + k\mathbf{b}^* + l\mathbf{c}^* + m\mathbf{q}$, denotes the four-dimensional lattice vector, where $\mathbf{q}$ is the wavevector of modulated wave. Here all atoms contribute to the structure modulation. If the displacement function is sinusoidal, then

$$\mathbf{u}_j = \mathbf{u}_{0j} \sin(2\pi \mathbf{q}.\mathbf{v} + \alpha). \quad (6)$$

Here $\mathbf{v}$ is the coordinate vector in fourth-dimensional real space. Substituting (6) into (5) gives

$$F(hklm) = A_m \sum_j f_j \exp 2\pi i(hx_j + ky_j + lz_j) J_m(2\pi \mathbf{g}.\mathbf{u}_{0j}), \quad (7)$$

where $J_m(x)$ is a Bessel function of order m and A_m is a phase factor.

From formula (7) it is seen that $F(hklm) = 0$ when $F(hkl0) = 0$. This means that if any main diffraction is prohibited by the extinction rule, then its satellite spots will also be prohibited. In this sense Figs. 2 and 3 are in agreement with (7) and hence support displacive rather than compositional modulation.

Based on the chemical formula of ankangite, there is less than one Ba atom in each unit cell but there are two positions for cations inside the tetragonal channels. Hence, the number of vacancies in the tetragonal channels is larger than the number of Ba atoms. Suppose that the idealized occupancy of the tetragonal channels in ankangite gives Ba–vacancy–Ba–vacancy sequences as proposed for hollandite by Dryden & Wadsley (1958). The additional vacancies would make Ba atoms deviate from their idealized positions and the translational order of the Ba atoms breaks down. The existence of sharp satellite diffraction indicates that the degree of deviation of the Ba atoms from their idealized positions must be controlled by a modulated wave to form the displacive modulated structure. This kind of displacive modulated structure, caused by the existence of vacancies, will be called a vacancy-displacive incommensurately modulated structure.

There are two typical types of displacive modulation, one is longitudinal wave modulation, for which the displacement of the atoms is parallel to the modulation wavevector, namely $\mathbf{u}_{0j} \| \mathbf{q}$; the other is transverse wave modulation, for which the displacement is normal to the modulation wavevector or $\mathbf{u}_{0j} \perp \mathbf{q}$. Since the modulation wavevector is parallel to the [001] direction in the case of a one-dimensional displacive modulated structure of the transverse type, for $00lm$ reflections the Bessel function in (7) should be

$$J_m(2\pi \mathbf{g}.\mathbf{u}_{0j}) = J_m[2\pi(l\mathbf{c}^* + m\mathbf{q}).\mathbf{u}_{0j}] = J_m(0) = 0 \ (m \neq 0). \quad (8)$$

Substitution of (8) into (7) gives

$$F_T(00lm) = 0. \quad (9)$$

Equation (9) suggests that for all main reflections of type 001 there will be no satellite spots. Obviously, this is contradictory to the EDP's given in Figs. 2(b) and 2(c). In the case of the longitudinal modulation wave the function

$$J_m(2\pi \mathbf{g}.\mathbf{u}_{0j}) = J_m 2\pi \mathbf{u}_{0j}.(\mathbf{H} + m\mathbf{q}),$$

will generally not equal zero. By substituting (8) into (6) it can be seen that all allowed main diffraction spots must be followed by satellite spots. This result is supported by Figs. 2(b) and 2(c).

Therefore, ankangite should have an incommensurate vacancy-displacive modulated structure with a longitudinal modulation wave. Ba ions deviate from their idealized positions along the c axis to form the longitudinal modulation wave.

Fig. 5(a) is a high-resolution electron microscopic image taken along the a axis. Fig. 5(b) is a local image magnified from Fig. 5(a). Figs. 5(c) and 5(d) are the corresponding EDP and optical diffraction pattern (ODP), respectively. Two kinds of rows of vertical white dots, consisting of large and small white dots, are arranged alternately in the image. The small dots do not have translational order along the [001] direction, while large white dots are arranged more or less periodically in comparison with the small dots. This can be seen more clearly in

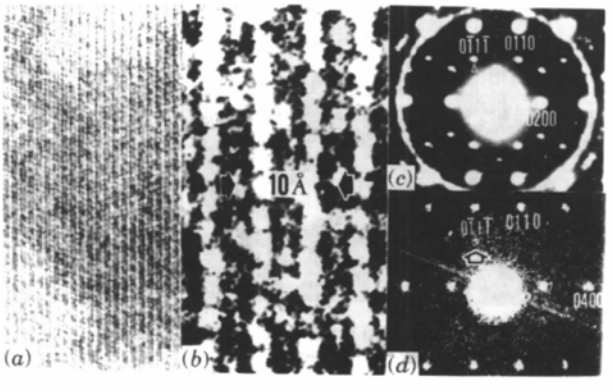

Fig. 5. (a) High-resolution image taken along the a axis, (b) enlarged photograph from (a), (c) corresponding electron diffraction pattern, and (d) optical diffraction pattern.

Fig. 5(*b*). Although the optical diffractograms are usually noisy, some satellite spots can still be distinguished in Fig. 5(*d*), such as the spot $0\bar{1}1\bar{1}$. This implies that the image does carry some structural information contributed by the satellite spots. In general, it can be assumed that the large white dots are mainly contributed by the main diffraction beams and show the lattice of the average structure, while the small white dots are mainly from the satellites and show the structure modulation. The fact that the image does not show any of the expected contrast corresponding to the modulated wave can be explained by the incoherency of Ba-ion strings, which also causes the diffraction streaks that can be seen in all of the EDP's. This will be discussed in more detail in §6.

It should be pointed out that the vacancy-displacive incommensurately modulated structure model is nothing to the local-ordered intergrowth model which was proposed by Bursill & Grzinic (1980) for hollandite.

6. Incoherency of Ba-ion strings in adjacent channels

In general, continuous planes in reciprocal space are due to thin needle-shaped crystals in real space. In the case of ankangite the continuous planes can be interpreted in terms of the existence of incoherent Ba-ion strings. Although the interaction between Ba ions located in the same tetragonal channel is very strong such that the Ba-ion strings have long-range order controlled by the modulated wave, the interaction is very weak for Ba-ion strings in different channels. Therefore, in some places the adjacent Ba-ion strings are incoherent to one another. This can be seen intuitively from the high-resolution images taken under special imaging conditions.

Fig. 6(*a*) is a lattice image taken along the *a* axis but under a much more divergent incident beam than usual. Although the corresponding EDP (Fig. 6*c*) is the same as Fig. 5(*c*), the corresponding ODP (Fig. 6*d*) is significantly different from Fig. 5(*d*). Fig. 6(*d*) indicates that the contrast of the image shown in Fig. 6(*a*) is contributed only by main reflections of type 0200 and satellites of type 0001. Hence, it is rather different from that in Fig. 5(*a*) which is contributed by more main reflections and satellites than in Fig. 6(*a*).

Since the main reflections 0010 and $00\bar{1}0$ are prohibited and the spacing of $d(002)$ is beyond the limit of the electron microscope, the contribution of sharp satellite spots of type 0001 to the image given in Fig. 6(*a*) should clearly show the periodicity of the modulated wave. However, only in some local regions of Fig. 6(*a*) do the white dots seem to be

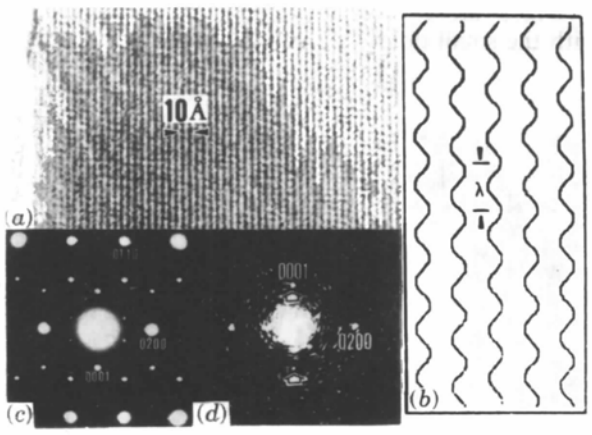

Fig. 6. (*a*) High-resolution image taken along the *a* axis but under a much more divergent incident beam than usual, (*b*) a schematic graph showing the modulated waves spreading along different atomic columns of Ba with different initial phases, (*c*) corresponding electron diffraction pattern, and (*d*) optical diffraction pattern.

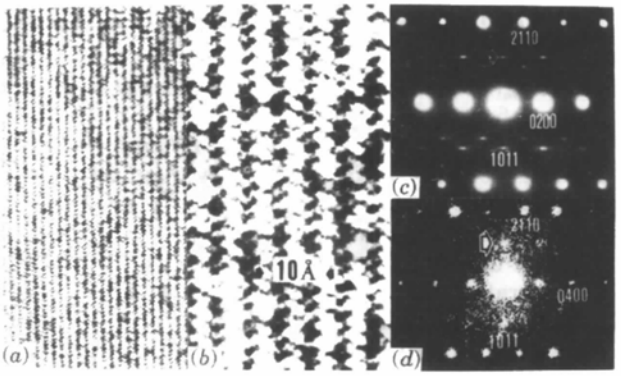

Fig. 7. (*a*) High-resolution image taken along $[10\bar{2}]$ before strong electron-beam irradiation, (*b*) enlarged photograph from (*a*), (*c*) corresponding electron diffraction pattern and (*d*) optical diffraction pattern.

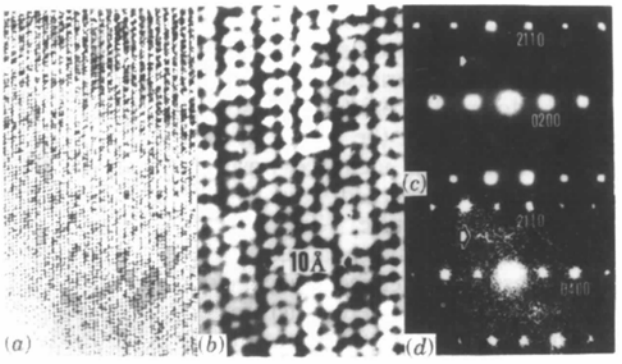

Fig. 8. (*a*) High-resolution image taken along $[10\bar{2}]$ after strong irradiation, (*b*) enlarged photograph of (*a*), (*c*) corresponding electron diffraction pattern and (*d*) optical diffraction pattern. The differences between this figure and Fig. 7 are very clear either in the images or in the diffraction patterns.

arranged in approximately horizontal rows, the distance between two rows being roughly equal to the wavelength of the modulated wave. This is due to the contribution of diffraction streaks, although these streaks cannot be distinguished from the noisy optical diffraction pattern. The image contrast is in agreement with the conclusion from the electron diffraction analysis and implies that the Ba-ion strings are incoherent to one another. The Ba ions with their idealized positions in the same plane parallel to the *ab* plane have different degrees of displacement along the *c* axis. In other words, the initial phases of the modulated waves spreading along the different atomic columns of Ba are different. Fig. 6(*b*) shows schematically the random phase shift of the modulated waves propagating along different tetragonal channels.

7. Effect of electron-beam irradiation

Fig. 7(*a*) is a high-resolution image taken along the $[10\bar{2}]$ direction and Fig. 7(*b*) is a local image magnified from Fig. 7(*a*); Figs. 7(*c*) and 7(*d*) are the corresponding EDP and ODP, respectively. The white dots in Figs. 7(*a*) and 7(*b*) are arranged almost periodically, but in fact there is no translational periodicity at all if the intensity of the white dots is taken into consideration. In the corresponding ODP shown in Fig. 7(*d*), besides the main diffraction spots the satellite spot $\bar{1}0\bar{1}1$ (indicated by an arrow) and the satellite spot $101\bar{1}$ can be seen clearly but the modulation contrast cannot be seen. This can also be interpreted in terms of the incoherency among different atomic columns of Ba. In any case, owing to the contribution of the satellite spots, including spots $\bar{1}0\bar{1}1$ and $101\bar{1}$, the image only shows a rough periodicity along the vertical direction. The vertical intensity change of the dots located in the same horizontal line is not synchronous.

After strong electron-beam irradiation, the images taken along the $[10\bar{2}]$ direction and the corresponding electron and optical diffraction patterns are shown in Fig. 8. There are no evident differences between corresponding main diffraction spots in Figs. 7(*c*) and 8(*c*), but the intensity of the satellite spots decreases greatly in Fig. 8(*c*). In Fig. 8(*b*) the white dots become more ordered in comparison with Fig. 7(*b*). This indicates that under electron-beam irradiation the incommensurate structure of ankangite tends towards a commensurate structure.

References

AXE, J. D. (1980). *Phys. Rev. B*, **21**, 4181–4190.

BEYELER, H. U. (1976). *Phys. Rev. Lett.* **37**, 1557–1560.

BURSILL, L. A. & GRZINIC, G. (1980). *Acta Cryst.* B**36**, 2902–2913.

BYSTROM, A. & BYSTROM, A. M. (1950). *Acta Cryst.* **3**, 146–154.

BYSTROM, A. & BYSTROM, A. M. (1951). *Acta Cryst.* **4**, 469.

DRYDEN, J. S. & WADSLEY, A. D. (1958). *Trans. Faraday Soc.* **54**, 1574–1580.

POST, J. E. & BURNHAM, C. W. (1986). *Am. Mineral.* **71**, 1178–1185.

POST, J. E., VON DREELE, R. B. & BUSECK, P. R. (1982). *Acta Cryst.* B**38**, 1056–1065.

SINCLAIR, W., MCLAUGHLIN, G. M. & RINGWOOD, A. E. (1980). *Acta Cryst.* B**36**, 2913–2918.

STEEDS, J. W., BIRD, D. M., EAGLESHAM, D. J., MCKERNAN, S., VINCENT, R. & WITHERS, R. (1985). *Ultramicroscopy*, **18**, 97–130.

WOLFF, P. M. DE (1974). *Acta Cryst.* A**30**, 777–785.

ZHOU, J. & MA, Z. S. (1987). *Geoscience*, **1**, 77–83.

Acta Cryst. (1990). B**46**, 117–125

Coincidence Orientations of Crystals in Tetragonal Systems, with Applications to $YBa_2Cu_3O_{7-\delta}$

BY A. SINGH, N. CHANDRASEKHAR AND A. H. KING

Department of Materials Science and Engineering, State University of New York at Stony Brook, Stony Brook, NY 11794-2275, *USA*

(*Received* 10 *April* 1989; *accepted* 21 *September* 1989)

Abstract

We have developed a method for the characterization of coincidence-site lattices (CSL's) in tetragonal or near-tetragonal orthorhombic structures, by suitable modifications to the method of Grimmer & Warrington [*Acta Cryst.* (1987), A**43**, 232–243]. We have applied our method to determine coincidence rotations and the associated information appropriate for forming constrained CSL's in the high-T_c superconductor $YBa_2Cu_3O_{7-\delta}$. The unit cell is orthorhombic with lattice parameters $a = 3{\cdot}82$, $b = 3{\cdot}89$

0108-7681/90/020117-09$03.00